Research Article

Cornelius Satria Yudha, Anjas Prasetya Hutama, Mintarsih Rahmawati, Meidiana Arinawati, Harry Kasuma (Kiwi) Aliwarga, Hendri Widiyandari and Agus Purwanto*

Production of nickel-rich $LiNi_{0.89}Co_{0.08}Al_{0.03}O_2$ cathode material for high capacity NCA/graphite secondary battery fabrication

https://doi.org/10.1515/eng-2022-0051
received October 23, 2021; accepted April 27, 2022

Abstract: Li-ion secondary battery is highly recommended as a power source to highly advanced battery electric vehicles. Among various types, the lithium nickel cobalt aluminum oxide (NCA) battery is considered suitable for high energy and power application. In this study, the NCA cathode material $LiNi_{0.89}Co_{0.08}Al_{0.03}O_2$ was produced via the oxalate co-precipitation technique to reduce the overall production cost and process complexity. Oxalic acid and a small amount of sodium hydroxide were used as the precipitant and pH regulator, respectively. Homogenous and loose metal oxalate precipitate formation was confirmed by X-ray diffraction (XRD), scanning electron microscopy, and Fourier-transform infrared spectroscopy analysis. XRD patterns of the as-obtained micron-sized NCA showed a well-layered hexagonal structure. The electrochemical properties of the cathode in the full cell were thoroughly examined. The specific discharge capacity of the as-obtained NCA in NCA/$LiPF_6$/graphite at a current rate of 20 mA/g was 142 mAh/g. The as-prepared NCA sample had capacity retention of 80% after being charged and discharged at 0.1 A/g for 101 cycles. Scaling up of NCA production process to 2 kg per batch was conducted and evaluation of NCA product quality was performed by material characterization. Based on the overall results and considering the overall process, such an approach is expected to be developed and improved for future large-scale production purposes.

Keywords: Li-ion batteries, co-precipitation, powder, NCA, cathode

1 Introduction

A layered type lithium nickel cobalt aluminum oxide (NCA) is considered as one of the promising and state-of-the-art cathode materials for Li-ion batteries (LIBs), owing to its excellent properties such as high columbic capacity, gravimetric energy density, and power density [1]. Currently, NCA with high nickel content such as $LiNi_{0.815}Co_{0.15}Al_{0.035}O_2$ is preferable because nickel is less toxic and less costly than cobalt [2,3]. In addition, the Ni-rich cathode material has a higher capacity than high cobalt content $LiCoO_2$. As a result, NCA/graphite batteries are a strong power source candidate for highly advanced electric vehicles.

Several attempts have been made to fabricate NCA micro-powders. The most convenient method is through the solid-state approach, which is limited to mixing the decomposable precursor with the lithium source followed by high-temperature annealing [4,5]. Decomposable precursors such as the hydroxide precursor and nitrate precursor are considered expensive, as their use increases the overall production cost. A similar concept was applied with the sol–gel method and spray pyrolysis where decomposable precursors are necessary [6–9]. Co-precipitation

* **Corresponding author: Agus Purwanto,** Material and Cell Fabrication Unit, Centre of Excellence for Electrical Energy Storage Technology, Universitas Sebelas Maret, Surakarta 57146, Indonesia; Department of Chemical Engineering, Universitas Sebelas Maret, Jl. Ir. Sutami 36A, Surakarta 57126, Indonesia, e-mail: aguspurwanto@staff.uns.ac.id
Cornelius Satria Yudha: Material and Cell Fabrication Unit, Centre of Excellence for Electrical Energy Storage Technology, Universitas Sebelas Maret, Surakarta 57146, Indonesia; Department of Chemical Engineering, Universitas Sebelas Maret, Jl. Ir. Sutami 36A, Surakarta 57126, Indonesia
Anjas Prasetya Hutama, Mintarsih Rahmawati, Meidiana Arinawati: Material and Cell Fabrication Unit, Centre of Excellence for Electrical Energy Storage Technology, Universitas Sebelas Maret, Surakarta 57146, Indonesia
Harry Kasuma (Kiwi) Aliwarga: UMG IdeaLab Indonesia, Jl. Tangkas Baru Komplek Polri Blok E/2, Karet Semanggi, Setiabudi, South Jakarta, Jakarta 12930, Indonesia
Hendri Widiyandari: Material and Cell Fabrication Unit, Centre of Excellence for Electrical Energy Storage Technology, Universitas Sebelas Maret, Surakarta 57146, Indonesia; Department of Physics, Universitas Sebelas Maret, Jl. Ir. Sutami 36A, Surakarta 57126, Indonesia

techniques are commonly applied for synthesizing the mixed metal precursor because the processes are facile, simple, do not require complex apparatus, and can be easily scaled up [10–12]. The raw materials have easy availability especially sulfate and chloride salts. The as-obtained powders usually have homogenous atom distribution and identical morphology with narrow size distribution. Thus, the co-precipitation process is suitable for synthesizing NCA precursors [3,13,14].

By far, co-precipitation of Ni–Co–Al salt solution was performed by hydroxide precipitation using sodium hydroxide (NaOH) as precipitant and ammonia as chelating agents. However, hydroxide precipitation of Ni–Co–Al ions is hampered by the dissolution of Al ions in elevated pH level that can cause poor homogeneity and agglomerated primary particles that often result in poor shelf-life of LIBs [3,15,16]. During the precipitation process, Co ions can be oxidized if the atmosphere is not inert. On the other hand, hydroxide co-precipitation requires a high amount of ammonia that is considered dangerous for aquatic life. The presence of ammonia in the ingredient also creates several respiratory problems for humans. Carbonate co-precipitation was applied due to the fast formation of particles in mild pH conditions; however, it still required significant ammonia during the precipitation as the chelating agent and pH regulator [17]. In contrast, oxalate precipitation is considered promising, as oxalate ions can be a precipitant, chelating, and reducing agent all at once, which is highly favorable for the overall process. Since the use of oxalic acid decreases the pH significantly, the pH can be regulated by an alkaline solution such as NaOH, thus the use of ammonia is unnecessary [18].

Several efforts have been employed to produce NCA using oxalic acid as a precipitant. Wu et al. [19] performed Ni–Co–Al oxalate via the two-step co-precipitation process to obtain a micro-rod-shaped NCA. Qiu et al. [20] performed precipitation of NCA from acetate salts precursors; however, in the study, water was removed by evaporation instead of the simple filtration process. This study was conducted to produce Ni-rich NCA micropowders using simple, ammonia-free, one-step oxalate co-precipitation followed by heat treatments. As far as our concern, such technique has never been reported elsewhere and has never used to be applied for large scale production of NCA type layered transition oxide cathode material. In other words, the proposed technique is potentially adapted for ammonia free-mass production of high energy density LIBs cathode material. In addition, the as-prepared material was tested in full-cell configuration. Thus, the study provided strong evidence for material utilization in the LIBs industry.

2 Materials and methods

Lithium hydroxide monohydrate, EN grade nickel sulfate hexahydrate (Zenith, Brazil), cobalt sulfate heptahydrate (Rubamin, India), and aluminum sulfate octadecahydrate (Mahkota, Indonesia) were used as Li, Ni, Co, and Al sources, respectively. Oxalic acid dihydrate (YC Chemicals Ltd, China) and NaOH (Asahi, Japan) were used as the precipitant and pH regulator, respectively. All of the materials were used directly without any purification step.

A 1 M of a solution containing Ni:Co:Al with molecular ratio of 89:8:3 was continuously stirred in a glass beaker and heated at 60°C for 30 min. The 1.5 M of the oxalic acid solution was transferred to the beaker with vigorous stirring until a bright green precipitate was formed. The solution pH of 3–4 was obtained by the addition of the 4 M NaOH solution. After 120 min, the stirring and heating were stopped, and the precipitate settled after the stirring was stopped. The solution was removed and changed with deionized water. The precipitate was filtered and washed until the solution reached neutral. The precipitate (NCA-oxalate) was transferred to an oven overnight or until dried. The dried precipitate was mixed with $LiOH{\cdot}H_2O$ (Leverton, India), using a planetary ball mill, ensuring a precursor to Li ratio of 1:1.05. After mixing homogenously, the precursor was heated at 500°C for 6 h and calcined at 800°C for 20 h under an O_2 atmosphere. The as-prepared product was sieved to fine powder. Large-scale production of NCA with a capacity of 2 kg per batch was conducted using a similar technique.

The structure of NCA samples was examined by an MD-10 X-ray diffractometer (MTI, USA). The samples' surface properties were analyzed using Fourier transform infrared (FTIR) spectroscopy (Shimadzu, Japan) and scanning electron microscope (SEM) (JEOL. Japan). A galvanostatic charge–discharge test was performed in NCA/$LiPF_6$/graphite cylindrical cells where the as-obtained NCA was used as the cathode of the cells. The electrode was fabricated with a coating of slurry containing 90:4:6 of NCA:acetylene black (AB):polyvinyl difluoride (PVdF) on the surfaces of Al foils. The coated foils were dried in a vacuum oven. The dried cathode was ready to be assembled with the graphite-coated Cu foil. The details of cylindrical cell assembly were described elsewhere in our previous reports [16,21]. Water-based manufacturing of NCA counter electrode was also conducted with a slurry containing 89:6:3:1:1 of meso carbon microbeads:AB:carboxy-methyl cellulose (CMC):styrene-butadiene rubber (SBR):oxalic acid. AB, PVdF, CMC, and SBR were obtained from MTI, USA. The manufactured cell was charged and discharged using 1/10 C (1 C = 0.2 A/g) the current rate at

the working voltage of 3.0–4.3 V using Neware Battery Analyzer (Neware, China) and BTS 7.6 Software. The cycle performance test was conducted using various charge–discharge rates (1 C = 200 mA/g), without any temperature control.

3 Results and discussions

3.1 Precipitation of NCA-oxalate

To assure the formation of the oxalate precipitate of NCA, the dried precipitate was analyzed using X-ray diffraction (XRD) and FTIR. Figure 1(a) displays the XRD patterns of the precipitate. The XRD peaks can be attributed to the nickel oxalate dihydrate compound, while the Miller indices are provided in the figure. The peaks observed are highly crystalline indicated by the sharp peaks on the pattern. The lattice parameter of NCA-oxalate powder is listed in Table 1. The *a*, *b*, and *c* values of the sample are almost similar with nickel oxalate dihydrate reference or Joint committee on the Powder Diffraction Standards (JCPDS) card no. 25-0582 [22], whereas the slight differences can be attributed to the presence of Co and Al atoms in the crystal structure. The lattice parameter values can be determined by linear regression of equations (1)–(3):

$$d_{hkl} = \frac{n \quad \lambda}{2 \quad \sin\theta}, \tag{1}$$

$$\frac{1}{d_{hkl}^2} = \frac{h^2}{a^2} + \frac{k^2}{b^2} + \frac{l^2}{c^2}, \tag{2}$$

$$V = a \times b \times c. \tag{3}$$

Based on Figure 1(b), infrared absorption patterns also confirm the presence of oxalate due to the O–C–O vibration located at a wavelength of 1,300 and 1,635 cm^{-1}. The hydrated crystal of oxalate is detected due to the presence of bending vibration of –OH at a wavelength of about 3,400 cm^{-1}. Thus, we can conclude that oxalate precipitation was successfully conducted [23].

The morphology of NCA-oxalate particles is depicted in Figure 2(a and b). The as-prepared NCA-oxalate powders are loose, irregular, or quasi-cubical shaped with smooth surfaces. The edges of the particles as well as the grains can be observed. It is safe to say that the particles have a homogenous shape with a size range of 1–3 μm. Figure 2(c) shows the EDX analysis of NCA-oxalate. It also can be seen that the sample has high Ni content and small Co and Al content. It can be concluded that aluminum ions can be precipitated during the co-precipitation due to mild pH solution (~4) where Al ion precipitation is possible in the form of aluminum hydroxide [24,25]. A small amount of S can be attributed to the

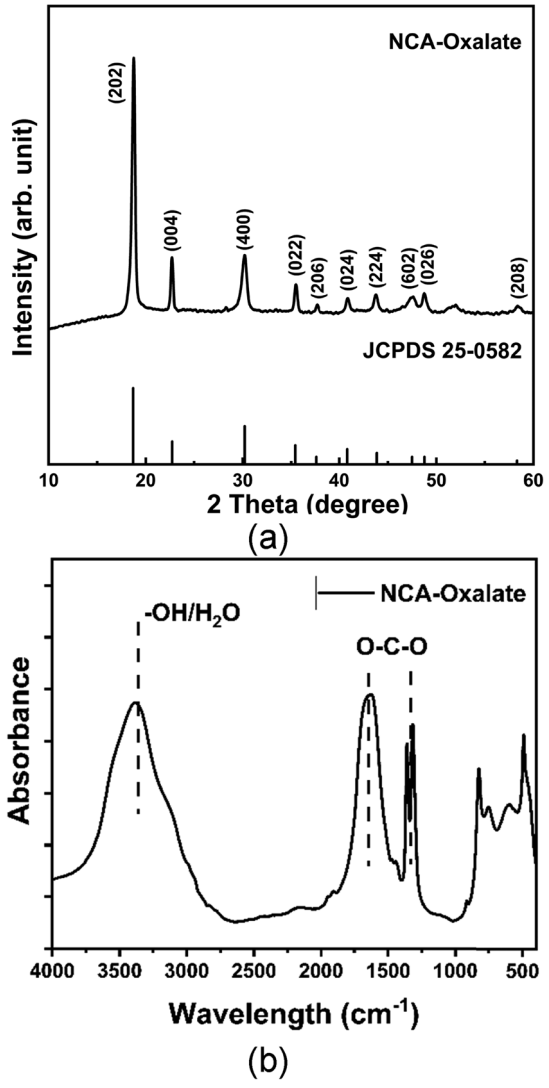

Figure 1: (a) X-ray diffractogram of NCA-oxalate and (b) modified FTIR spectra of NCA-oxalate.

Table 1: Lattice parameter and structural parameter of the as-prepared NCA-oxalate

Parameters	Value	Ref. $NiC_2O_4{\cdot}H_2O$ [22]	Unit
Lattice			
• *a*	11.837	11.762	Å
• *b*	5.342	5.332	Å
• *c*	15.623	15.726	Å
• Lattice volume	988.007	986.256	$Å^3$

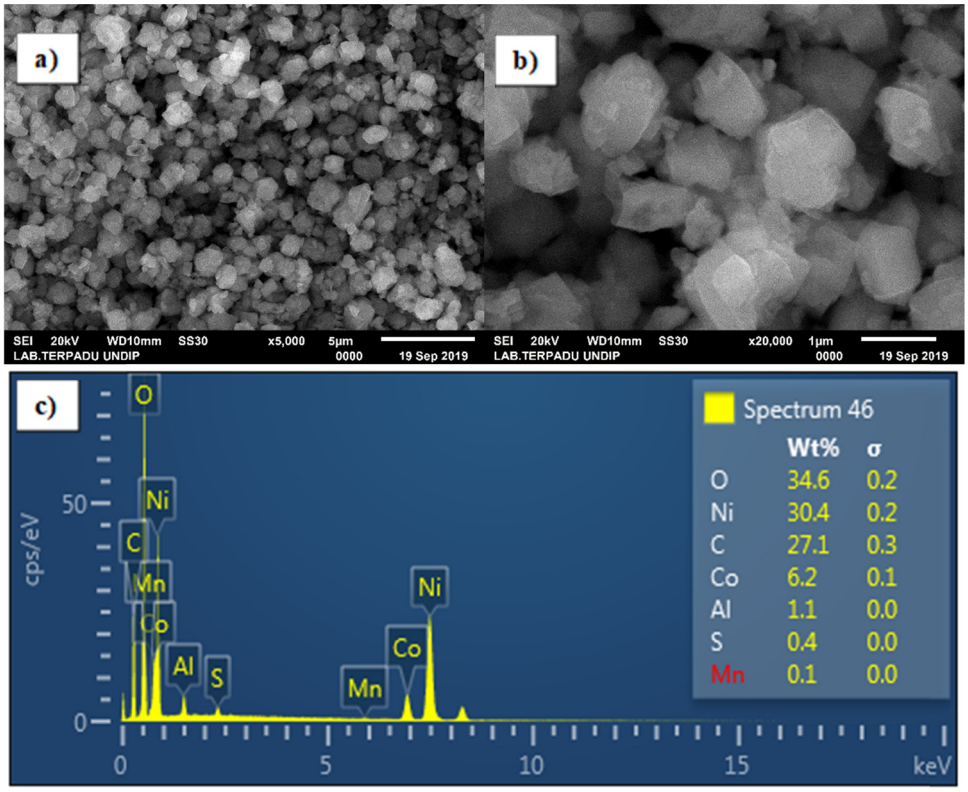

Figure 2: SEM images and EDX analysis of NCA-oxalate (a)–(c).

presence of sulfate while the presence of Mn can be attributed to the low-quality grade of metal sulfate salt precursors.

3.2 $LiNi_{0.89}Co_{0.08}Al_{0.03}O_2$ (NCA) characterization

In this study, $LiNi_{0.89}Co_{0.08}Al_{0.03}O_2$ powder was obtained by a high-temperature lithiation of the NCA precursor. Figure 3(a) displays the X-ray diffractogram of as-prepared NCA. The peaks observed in Figure 3(a) are well indexed to the JCPDS card no. 87-1562 where the Miller indices are displayed as shown in the figure, with no impurities detected. It can be concluded that the material has a layered structure with the hexagonal ordering of atoms [26,27]. Peak doublets splitting of (006/102) and (018/110) are observed, which is based on previous studies. The appearance of these peaks on a layered structure cathode material means that the material has a good structural property, which favors the lithium transfer process when applied to LIBs cells [15,28]. The formation or the unsuccessful oxidation of Ni^{2+} brings a negative effect on the NCA electrochemical performance. The similar atomic radii of Ni^{2+} and Li^{+} often cause a cation mixing phenomenon in the structure lattice. The presence of Ni^{2+} in the Li layer forms a blockade that prevents Li-ion mobility during the charge–discharge process. The level of cation mixing of layered material can be evaluated by the intensity ratio of peaks (003) and (104) or $I(003)/(104)$. From Figure 4, we can also conclude that as-prepared NCA powder has a low tendency to form cation displacement of Li and Ni or cation mixing, owing to the peak intensity ratio (103)/(104) value of over 1.3 [28,29].

Figure 3(b) exhibits the IR absorbance spectra of NCA. The slightly observed peak at a wavenumber of around 3,400 cm^{-1} can be attributed to the presence of water molecules in the sample [30]. Nickel-rich cathode material such as NCA is hygroscopic; therefore, this phenomenon occurred due to water absorption on the surface of the NCA particle due to humidity. Observed peak doublets at approximately 1,600 cm^{-1} indicate the existing residual and unreacted Li in the form of Li_2CO_3, which exist due to excess lithium added during the high-temperature lithiation process. However, from both Figure 3(a) and (b), we can conclude that the well-indexed, layered structure of NCA powder is successfully synthesized and the lattice and structural parameters are listed in Table 2 [16,31].

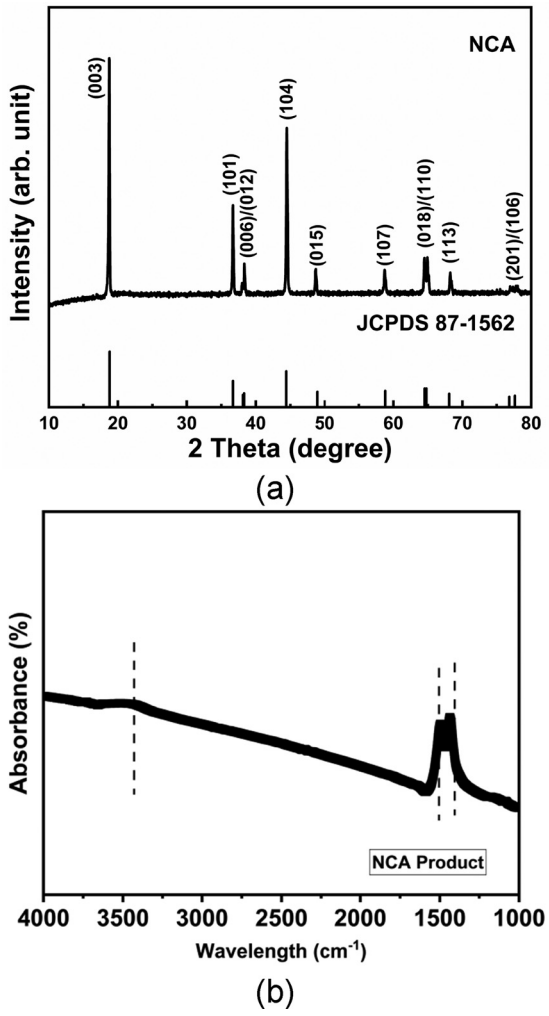

Figure 3: (a) X-ray diffractogram and (b) modified FTIR spectra of as-prepared NCA powder.

The as-prepared NCA particles can be seen in Figure 4. The particles have clear edges and a slightly smooth surface. After a sintering process at a high temperature, the morphology of the particles is sustained from its original form of NCA-oxalate, even though CO_2 was decomposed during the calcination process, leaving porous particles, as described by Qiu et al. However, high-temperature sintering may remove the porous particles into dense particles [20].

Table 2: Lattice parameter and structural parameter of the as-prepared NCA powder

Parameters	Value	Unit
Lattice		
• *a*	2.867	Å
• *c*	14.177	Å
• *c/a*	4.945	Å
• Lattice volume	302.755	$Å^3$
Structure		
• *I* ratio	1.409	—
• *R*-value	0.306	—
• Crystallite size	55	nm

3.3 Galvanostatic charge–discharge performance of the NCA in NCA/$LiPF_6$/graphite battery

Charge–discharge analysis of as-prepared NCA powders was conducted in anode-free Li-ion batteries (AFLIB) and full battery design where the cathode material is the as-prepared NCA. Bare Cu foil was used for Li-plating during the charging process of AFLIB. Graphite was utilized as the anode where the theoretical capacity was designed in excess; therefore, the mass of NCA was selected as the basis of weight for calculating specific capacity. About 1 M $LiPF_6$ dissolved inhomogeneous mixture of 1:1 dimethyl carbonate and ethyl carbonate was used as the aprotic electrolyte. The charge–discharge profile of

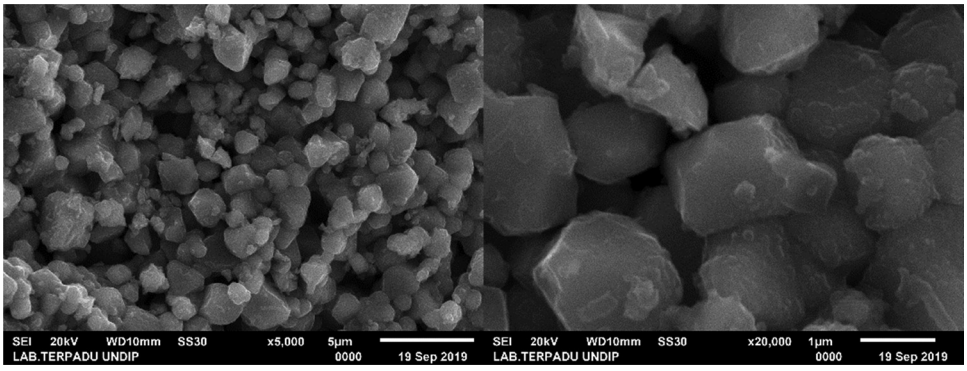

Figure 4: SEM images of NCA powder.

the NCA/$LiPF_6$/Cu and NCA/$LiPF_6$/graphite cells can be seen in Figure 5. In the first cycle, during the charging process, the Li-ions were transferred from the cathode lattice to the counter electrode. The voltage was initially zero and then started to elevate as more Li-ions were transferred. In Figure 5a, the voltage of the cell increased rapidly at ~3.8 V which indicates an initial Li-plating of Li-ion on the surface of Cu foil. The initial charge–discharge capacity of NCA in AFLIB is 216 and 149 mAh/g, respectively. In the second cycle, the capacity improved to above 153 mAh/g while in the sixth cycle, the capacity significantly decreased. This indicates that during the initial charge, some of the material is still inactive while in the sixth cycle the decay was caused by dead Li formation often found in AFLIB [32]. After the cell reached 4.3 V, the cells are discharged where the Li-ions are transferred from the anode back to the cathode. Thus, such a phenomenon is often called the rocking chair mechanism [33]. From Figure 5b, in the first cycle, the specific charge capacity is also larger than the discharge capacity. The initial capacity loss can be attributed to the formation of solid electrolyte interphase (SEI), where some of the Li is deposited on the surface of the anode, which disabled its mobility to return to the cathode during discharge. However, in the second cycle and the sixth cycle, the specific charge capacity and the specific discharge capacity are equal, where the columbic efficiency value is approaching almost 100%. The initial discharge capacity of NCA is 142 mAh/g operated at a charge–discharge current of 20 mA/g and voltage window of 3.0–4.3 V. The capacity is lower compared to several studies. This can be caused by several factors. For instance, the nickel content in this research is significantly higher. Higher Ni content material is often hard to oxidize and suffers from the formation of electrochemically inactive phase. Secondly, the morphology can be a factor since nickel-rich cathode is highly sensitive towards side reactions with the electrolyte, especially particles with small size and large surface area. However, this result is considered good, considering that the overall process is simple, cheap, fast, and less harmful for the environment due to the absence of ammonia.

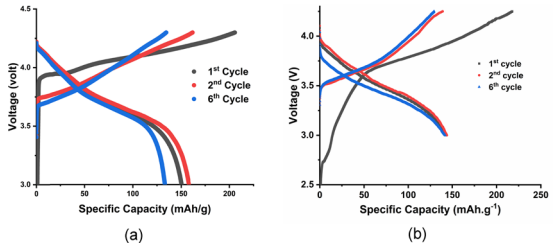

Figure 5: Charge–discharge profile of (a) NCA/$LiPF_6$/Cu AFLIB and (b) full cell NCA/$LiPF_6$/graphite cells.

Figure 6(a) exhibits the cycle performance of the NCA/$LiPF_6$/graphite cells under the current rate of 1/2 C (100 mAh/g) with the operating voltage of 3.0–4.3 V. Based on the figure, the cells have columbic efficiency of about 100%, which indicates good Li-ion reversibility. However, after 100 cycles, a capacity drop can be observed clearly. At a current of 1/2 C, the specific discharge capacity of the cell is about 130 mAh/g, which is 91% compared to the capacity tested at 1/10 C. In the 101st cycle, the specific discharge capacity of the cell is about 105 mAh/g, which is 80.1% compared to the starting capacity. The capacity retention profile is displayed in Figure 6(b) [34]. The reduction of capacity occurred significantly in the first 20 cycles; however, in the 21st cycle the curve shows better capacity. The rapid capacity decay at early cycles may be caused by the existence of residual Li, particularly Li_2CO_3 which is confirmed by a previous FTIR study. Li_2CO_3 presence can promote the formation of HF which can severe the NCA particle [35]. The accumulated coulombic inefficiency in Figure 3c shows that the curve is consistently increasing which is consistent with the cycle performance which also shows a relatively consistent capacity decrease [36]. The rate ability of NCA displayed in Figure 6d indicates that NCA is still operable at an elevated current of 1, 2, 4, and 8 C with an average discharge capacity of 123, 101, 80, and 28 mAh/g, respectively. The NCA still has a capacity of 121 mAh/g when charged and discharged at 1 C which proves that the cell has good reversibility.

3.4 Preliminary demo-plant-scale production of $LiNi_{0.89}Co_{0.08}Al_{0.03}O_2$

A 100-time multiplication of previous lab-scale production was conducted. About 2 kg of NCA product was synthesized and characterized. The production facility can be seen in Figure 7(a). The NCA precursor solution was reacted with NaOH and oxalic acid in a continuously stirred reactor. The slurry was filtered and washed using a centrifugal filter and the cake was dried in a vacuum oven. The precursor was milled with LiOH using a ball mill machine, then the composite was fired in a large muffle furnace under O_2 flow. The characterization of NCA-oxalate and NCA products produced at 1 kg/batch scale, labeled as NCA-OLS and NCA-LS, respectively, can be seen in Figure 7(b–e). Figure 7(b) shows the FTIR spectra of NCA-oxalate and NCA products. Based on the figure, NCA-oxalate dihydrate was successfully

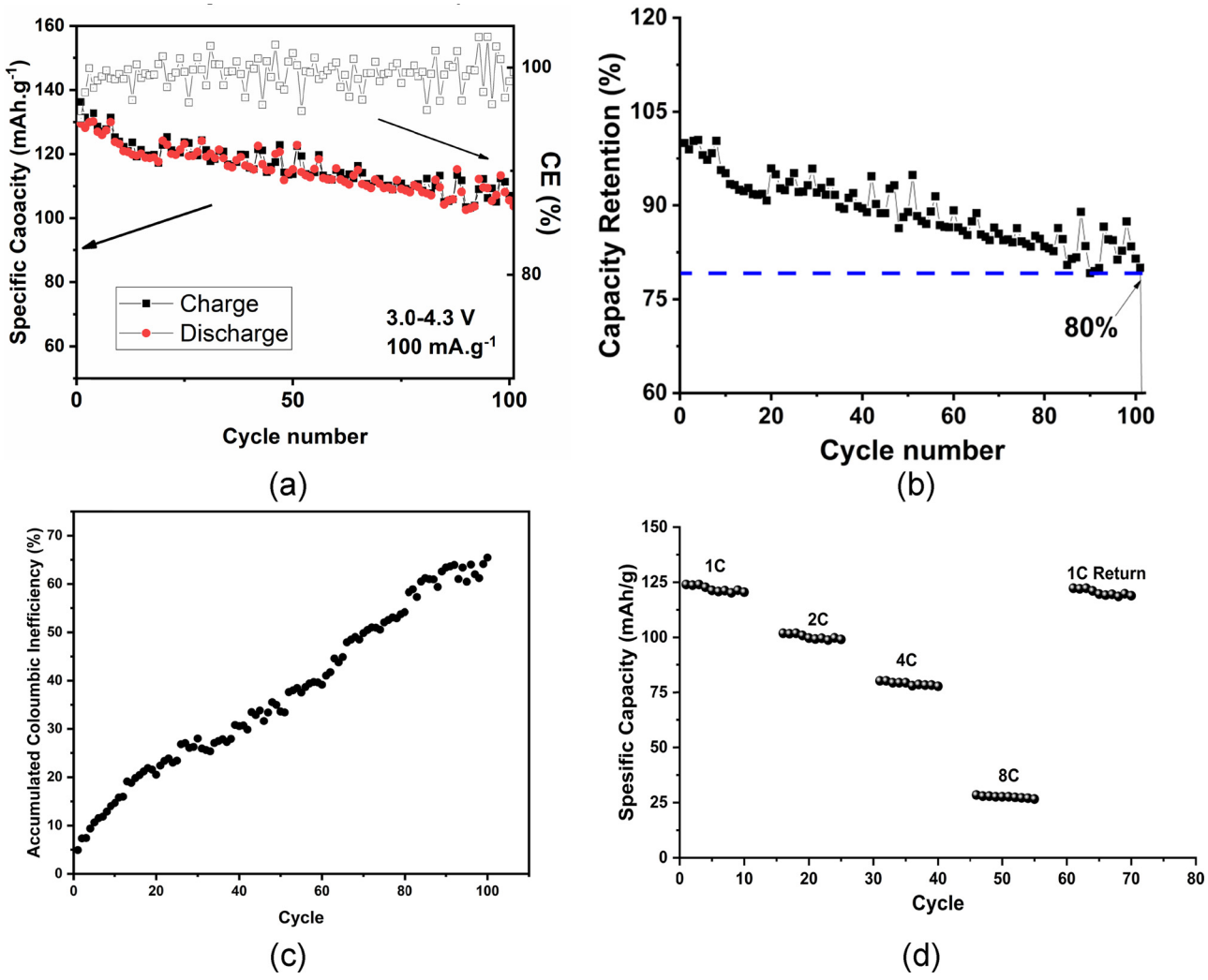

Figure 6: (a) Cycle performance, (b) capacity retention profile, (c) accumulated coloumbic inefficiency, and (d) rate ability of NCA/$LiPF_6$/graphite cells.

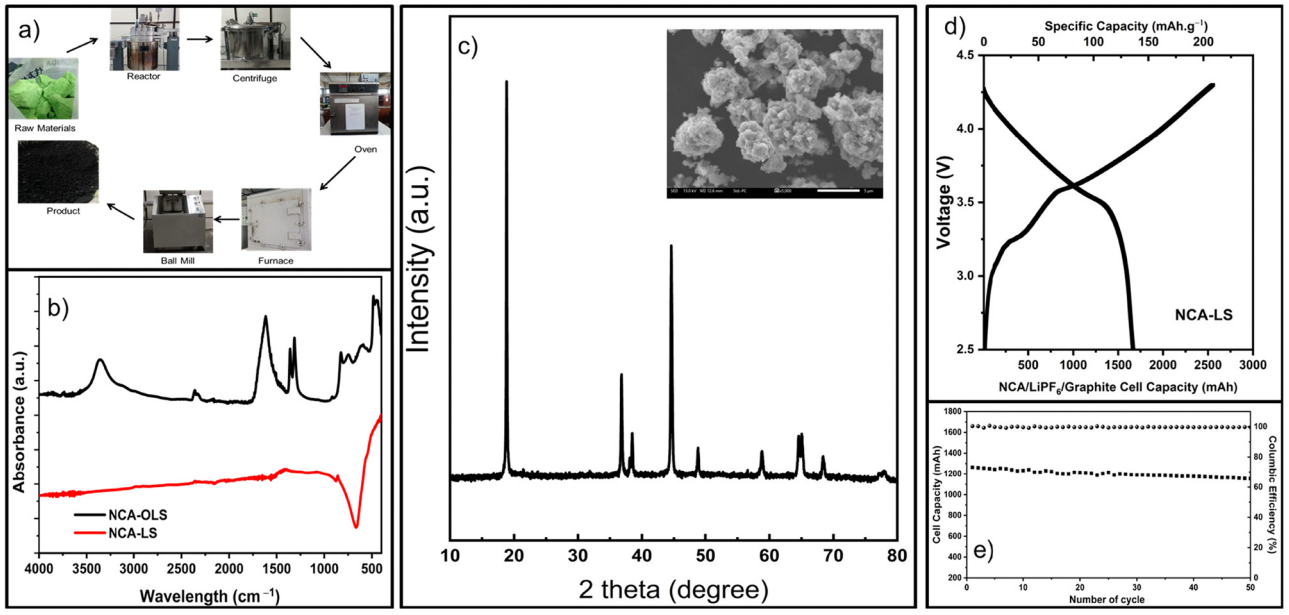

Figure 7: (a) Flow diagram of 2 kg per batch of NCA production and product (NCA-LS) characterization by (b) FTIR, (c) XRD/SEM, (d) charge–discharge performance test, and (e) cycle performance test.

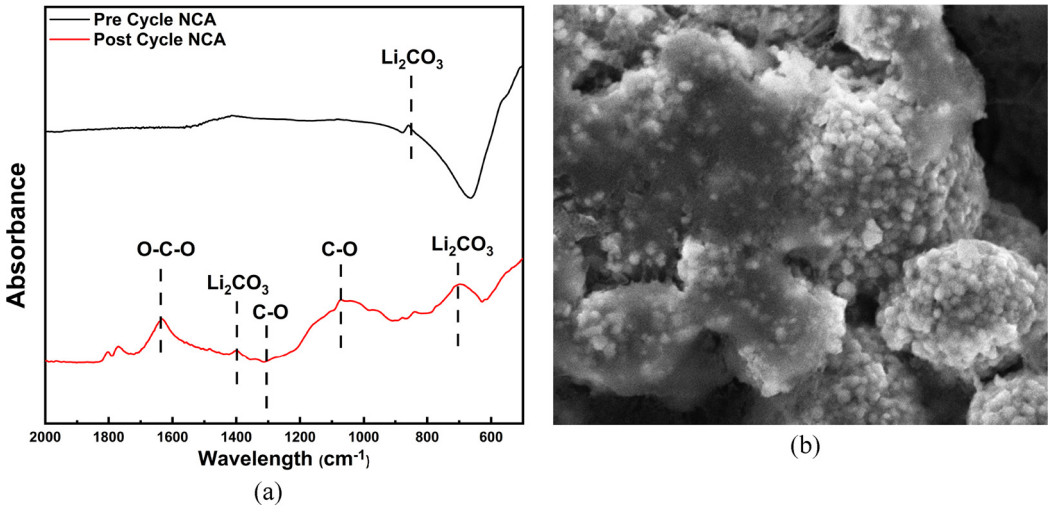

Figure 8: (a) FTIR and (b) SEM image of post-cycled NCA-LS.

synthesized as the patterns are identical with the pattern in Figure 1(b) while the NCA-LS FTIR spectra have lower CO_2 peaks due to isolated grinding and sieving process using a ball-mill machine thus less exposure to the atmosphere. Figure 7c shows the XRD pattern of NCA-LS while the SEM images can be seen in figure inset. The XRD peaks of NCA-LS are well indexed to NCA reference while the SEM image confirms that there is a significant difference of morphology between NCA-LS with NCA in Figure 4. The NCA-LS primary particles size is less than 1 µm which forms a large micron-sized secondary particle. The $I_{(003)}/I_{(104)}$ value is higher than NCA produced at the lab scale. Cell performance of NCA-LS is depicted in Figure 7(d and e). The initial specific charge and discharge capacity of NCA-LS is 210 and 136 mAh/g, respectively, which is lower than NCA produced at the lab scale. The lower capacity is considered normal since the production capacity was significantly increased. A large amount of processed material required a challenging parameter modification, especially to avoid cation mixing which often occurred in layered transitional metal oxide cathode material. This phenomenon always occurs in Ni-rich cathode material. The cycle performance was conducted at 1/2 C (100 mA/g) where the cell exhibited more stable performance owing to low cation disarrangement which was indicated by the *I* ratio value and less residual Li content on the surface of the material. The result is considered promising but it can be improved by optimization. Nevertheless, further research and deep investigation on process scale-up of NCA production are necessary to be performed shortly.

3.5 Post-mortem analysis of $LiNi_{0.89}Co_{0.08}Al_{0.03}O_2$ (NCA-LS)

A post-mortem analysis was conducted to investigate the condition of NCA material after cycled for 50 times. From the previous discussion, a capacity decay during the cycling test was unavoidable. The loss of active material during a cycling test, the loss of reversible lithium-ion, and impedance increase is the reason for capacity decay. FTIR studies of the post-cycled sample in Figure 8a show the occurrence of alkyl-oxide-lithium or ROLi, $ROCO_2Li$, and carbonate species as a result of organic electrolyte degradation. The SEM image in Figure 8b confirms the presence of the SEI layer on the surface of the NCA-post-cycle [37].

4 Conclusion

A simple oxalate co-precipitation technique was successfully applied to produce high Ni content of $LiNi_{0.89}Co_{0.08}Al_{0.03}O_2$ (NCA) cathode material of LIBs. Based on the XRD and FTIR analysis, a nickel-rich oxalate precursor was successfully formed by the reaction of a solution containing Ni, Co, and Al ions with oxalic acid. After the heating process, highly crystalline material with good structural property NCA powders was obtained, which was confirmed by XRD and FTIR analysis. The initial discharge capacity of the as-obtained NCA was 142 mAh/g, measured at a charge–discharge current of 1/10 C and voltage window

of 3.0–4.3 V. After 101 cycles at 1/2 C, the cell has a capacity retention of 80%. Scale-up production of NCA powder with a processing capacity of 2 kg per batch is conducted. The results are satisfying; however, there is room for many improvements. We can conclude that the overall process is promising to be further developed in the future.

Acknowledgment: The authors acknowledge financial support by UMG Idealab Indonesia.

Funding information: We also acknowledge Lembaga Penelitian dan Pengabdian Masyarakat (LPPM) Universitas Sebelas Maret for the support through Penelitian Fundamental (PF) grant no. 254/UN27.22/PT.01.03/2022.

Author contributions: Conceptualization, C. S. Yudha and A. Purwanto.; methodology, H. Widiyandari and C. S. Yudha; data curation, M. Rahmawati; writing—review and editing, C. S. Yudha and A. Purwanto.; supervision, H.K. Aliwarga. All authors have read and agreed to the published version of the manuscript.

Conflict of interest: The authors state no conflict of interest.

Data availability statement: The datasets generated during and/or analyzed during the current study are available from the corresponding author on reasonable request.

References

[1] Lie TT, Liang X, Haque MH. A cost-effective electric vehicle charging method designed for residential homes with renewable energy. Open Eng. 2015;5(1):166–78. doi: 10.1515/eng-2015-0022.

[2] Lai YQ, Xu M, Zhang ZA, Gao CH, Wang P, Yu ZY. Optimized structure stability and electrochemical performance of $LiNi_{0.8}Co_{0.15}Al_{0.05}O_2$ by sputtering nanoscale ZnO film. J Power Sources. 2016;309:20–6. doi: 10.1016/j.jpowsour.2016.01.079.

[3] Purwanto A, Yudha CS, Ubaidillah U, Widiyandari H, Ogi T. NCA cathode material: synthesis methods and performance enhancement efforts. Mater Res Express. 2018;5(12):122001. doi: 10.1088/2053-1591/aae167.

[4] Qiu Z, Zhang Y, Dong P, Xia S, Yao Y. A facile method for synthesis of $LiNi_{0.8}Co_{0.15}Al_{0.05}O_2$ cathode material. Solid State Ion. 2017;307(December 2016):73–8. doi: 10.1016/j.ssi.2017.04.011.

[5] Takanashi S, Abe Y. Improvement of the electrochemical performance of an NCA positive-electrode material of lithium ion battery by forming an Al-rich surface layer. Ceram Int. 2017;43(12):9246–52. doi: 10.1016/j.ceramint.2017.04.080.

[6] Yudha CS, Muzayanha SU, Rahmawati M, Widiyandari H, Sutopo W, Nizam M, et al. Fast production of high performance $LiNi_{0.815}Co_{0.15}Al_{0.035}O_2$ cathode material via urea-assisted flame spray pyrolysis. Energies. 2020;13:2757. doi: 10.3390/en13112757.

[7] Nurcahyani C, Anjani AE, Purwanto A, Yudha CS, Hasanah LM, Dyartanti ER, et al. Flame-assisted spray pyrolysis of lithium nickel cobalt aluminum oxide leaching stream. AIP Conf Proc. 2219, 2020;030003:1–9. doi: 10.1063/5.0003156.

[8] Jiang D, Zhao L, Shao Y, Wang D. Preparation and characterization of layered $LiNi_{0.9}Co_{0.05}Mn_{0.025}Mg_{0.025}O_2$ cathode material by a sol-gel method for lithium-ion batteries. RSC Adv. 2015;5(51):40779–84. doi: 10.1039/c5ra05669a.

[9] Chien WC, Li YR, Wu SH, Wu YS, Wu ZH, James Li YJ, et al. Modifying the morphology and structure of graphene oxide provides high-performance $LiFePO_4$/C/rGO composite cathode materials. Adv Powder Technol. 2020;31:4541–51. doi: 10.1016/j.apt.2020.10.002.

[10] Zheng M, Lu L, Sun S, Hu J, Teng H. Endothermic properties of modified expanded graphite-based $Ca_xZn_y(OH)_{2(x+y)}$ composite materials for heat storage. Open Eng. 2016;6(1):648–52. doi: 10.1515/eng-2016-0091.

[11] Arinawati M, Hutama AP, Yudha CS, Rahmawati M, Purwanto A. Facile rheological route method for $LiFePO_4$/C cathode material production. Open Eng. 2021;11(1):669–76. doi: 10.1515/eng-2021-0068.

[12] Zheng M, Sun SM, Hu J, Zhao Y, Yu LJ. Preparation of nanocomposite Ca_2-αZnα$(OH)_4$ with high thermal storage capacity and improved recovery of stored heat energy. Open Eng. 2015;5(1):42–7. doi: 10.1515/eng-2015-0002.

[13] Son JT, Jeon HJ, Lim JB. Synthesis and electrochemical characterization of Li_2MnO_3-$LiNi_xCO_yMn_zO_2$ cathode for lithium battery using co-precipitation method. Adv Powder Technol. 2013;24(1):270–4. Available from: doi: 10.1016/j.apt.2012.06.014.

[14] Purwanto A, Nisa SS, Lestari IP, Ikhsanudin MN, Yudha CS, Widiyandari H. High performance nickel based electrodes in state-of-the-art lithium-ion batteries: morphological perspectives. KONA Powder Part J. 2022;September:1–20. doi: 10.14356/kona.2022015.

[15] Muzayanha SU, Yudha CS, Nur A, Widiyandari H, Haerudin H, Nilasary H, et al. A fast metals recovery method for the synthesis of lithium nickel cobalt aluminum oxide material from cathode waste. Metals (Basel). 2019;9:9615. doi: 10.3390/met9050615.

[16] Yudha CS, Muzayanha SU, Widiyandari H, Iskandar F, Sutopo W, Purwanto A. Synthesis of $LiNi_{0.85}Co_{0.14}Al_{0.01}O_2$ cathode material and its performance in an NCA/graphite full-battery. Energies. 2019;12(10):1886. doi: 10.3390/en12101886.

[17] Seo J, Lee J. Fast growth of the precursor particles of Li$(Ni_{0.8}Co_{0.16}Al_{0.04})O_2$ via a carbonate co-precipitation route and its electrochemical performance. J Alloy Compd. 2017;694:703–9. doi: 10.1016/j.jallcom.2016.10.062.

[18] Sun L, Qiu K. Organic oxalate as leachant and precipitant for the recovery of valuable metals from spent lithium-ion batteries. Waste Manag. 2012;32(8):1575–82. doi: 10.1016/j.wasman.2012.03.027.

[19] Wu N, Wu H, Yuan W, Liu S, Liao J, Zhang Y. Facile synthesis of one-dimensional $LiNi_{0.8}Co_{0.15}Al_{0.05}O_2$ microrods as advanced

cathode materials for lithium ion batteries. J Mater Chem A. 2015;3(26):13648–52. doi: 10.1039/C5TA02767E.
[20] Qiu Z, Zhang Y, Xia S, Yao Y. A facile method for synthesis of $LiNi_{0.8}Co_{0.15}Al_{0.05}O_2$ cathode material. Solid State Ion. 2017;307(April):73–8. doi: 10.1016/j.ssi.2017.04.011.
[21] Purwanto A, Jumari A, Nizam M, Widiyandari H, Mohamad AA. Improving cylinder-type $LiFePO_4$ battery performance via control of internal resistance. Mater Res Express. 2018;5(4):45512. doi: 10.1088/2053-1591/aabddc.
[22] Oh HJ, Jo CH, Yoon CS, Yashiro H, Kim SJ, Passerini S, et al. Nickel oxalate dihydrate nanorods attached to reduced graphene oxide sheets as a high-capacity anode for rechargeable lithium batteries. NPG Asia Mater. 2016;8(5):e270. doi: 10.1038/am.2016.59.
[23] Jumari A, Nur K, Stulasti R, Halimah RN, Aini LA, Mintarsih R. Production of $LiNi_{0.6}Mn_{0.2}Co_{0.2.2}O_2$ via fast oxalate precipitation for Li-ion. In: The 5th International Conference on Industrial, Mechanical, Electrical, and Chemical Engineering 2019 (Icimece 2019). Published; 2020. p. 2–7. doi: 10.1063/5.0000646.
[24] He K, Ruan Z, Teng X, Zhu Y. Facile synthesis and electrochemical properties of spherical $LiNi_{0.85-x}Co_{0.15}Al_xO_2$with sodium aluminate via co-precipitation. Mater Res Bull. 2017;90:131–7. doi: 10.1016/j.materresbull.2017.01.039.
[25] Xie H, Du K, Hu G, Duan J, Peng Z, Zhang Z, et al. Synthesis of $LiNi_{0.8}Co_{0.15}Al_{0.05}O_2$ with 5-sulfosalicylic acid as a chelating agent and its electrochemical properties. J Mater Chem A. 2015;3(40):1–21. doi: 10.1039/C5TA05266A.
[26] Nakamura E, Kondo A, Matsuoka M, Kozawa T, Naito M, Koga H, et al. Preparation of $LiCoO_2/Li_{1.3}Al_{0.3}Ti_{1.7}(PO_4)_3$ composite cathode granule for all-solid-state lithium-ion batteries by simple mechanical method. Adv Powder Technol. 2016;27(3):825–9. doi: 10.1016/j.apt.2015.10.013.
[27] Kondo A, Nakamura E, Kozawa T, Abe H, Naito M, Yoshida J, et al. One-pot mechanical synthesis of the nanocomposite granule of $LiCoO_2$ nanoparticles. Adv Powder Technol. 2014;25(4):1280–4. doi: 10.1016/j.apt.2014.03.005.
[28] Li J, Zhang N, Li H, Liu A, Wang Y, Yin S, et al. Impact of the synthesis conditions on the performance of $LiNi_xCo_yAl_zO_2$ with high Ni and low Co content. J Electrochem Soc. 2018;165(14):A3544–57. doi: 10.1149/2.0931814jes.
[29] Zhang J, Xu S, Hamad KI, Jasim AM, Xing Y. High retention rate NCA cathode powders from spray drying and flame assisted spray pyrolysis using glycerol as the solvent. Powder Technol. 2020;363:1–6. doi: 10.1016/j.powtec.2019.12.057.
[30] Zhao F, Han F, Zhang S, Zhang Z. Vacuum drying characteristics of $LiNi_{0.5}Co_{0.2}Mn_{0.3}O_2$ battery powder. Adv Powder Technol. 2020;32:10–8. doi: 10.1016/j.apt.2020.11.003.
[31] Visbal H, Fujiki S, Aihara Y, Watanabe T, Park Y, Doo S. The influence of the carbonate species on $LiNi_{0.8}Co_{0.15}Al_{0.05}O_2$ surfaces for all-solid-state lithium ion battery performance. J Power Sources. 2014;269:396–402. doi: 10.1016/j.jpowsour.2014.07.021.
[32] Xie Z, Wu Z, An X, Yue X, Wang J, Abudula A, et al. Anode-free rechargeable lithium metal batteries: progress and prospects. Energy Storage Mater. 2020;32(July):386–401. doi: 10.1016/j.ensm.2020.07.004.
[33] Ito S, Fujiki S, Yamada T, Aihara Y, Park Y, Kim TY, et al. A rocking chair type all-solid-state lithium ion battery adopting $Li_2O–ZrO_2$ coated $LiNi_{0.8}Co_{0.15}Al_{0.05}O_2$ and a sulfide based electrolyte. J Power Sources. 2014;248:943–50. doi: 10.1016/j.jpowsour.2013.10.005.
[34] Purwanto A, Yudha CS, Ikhwan Muhammad K, Algifari BG, Widiyandari H, Sutopo W. Synthesis of $LiNi_{0.8}Co_{0.15}Al_{0.05}O_2$ cathode material via flame-assisted spray pyrolysis method. Adv Powder Technol. 2020;31(February):1–8. doi: 10.1016/j.apt.2020.01.035.
[35] Tang ZF, Wu R, Huang PF, Wang QS, Chen CH. Improving the electrochemical performance of Ni-rich cathode material $LiNi_{0.815}Co_{0.15}Al_{0.035}O_2$ by removing the lithium residues and forming Li_3PO_4 coating layer. J Alloy Compd. 2017;693:1157–63. doi: 10.1016/j.jallcom.2016.10.099.
[36] Holtstiege F, Wilken A, Winter M, Placke T. Running out of lithium? A route to differentiate between capacity losses and active lithium losses in lithium-ion batteries. Phys Chem Chem Phys. 2017;19(38):25905–18. doi: 10.1039/c7cp05405j.
[37] Liu C, Qian K, Lei D, Li B, Kang F, He Y-B. Deterioration mechanism of $LiNi_{0.8}Co_{0.15}Al_{0.05}O_2$/graphite–$SiO_x$ power batteries under high temperature and discharge cycling conditions. J Mater Chem A. 2018;6(1):65–72. doi: 10.1039/C7TA08703A.